Tang *et al. Biochar* (2026) 8:25
https://doi.org/10.1007/s42773-025-00530-7

Biochar

ORIGINAL RESEARCH Open Access

Enhancing the transformation of nitrogenous organics to humification in composting: biotic and abiotic synergy mediated by phosphorus and magnesium modified biochar

Ruolan Tang[1], Yan Liu[1], Jingyuan Ma[1], Sheng Yao[1,2], Tianyu Ren[1], Guoxue Li[1], Xiaoyan Gong[1], Ruonan Ma[1] and Jing Yuan[1*]

Abstract

This study developed phosphorus-modified biochar (BCP) and phosphorus-magnesium co-modified biochar (BCPM) to improve nitrogen retention and humification during composting. Systematically, this study elucidated the synergistic biotic-abiotic mechanisms by tracking nitrogen transformation, fluorescence spectral dynamics, functional genes and microbial succession. Results demonstrated that compared to conventional biochar (BC), the BCP/BCPM immobilized NH_4^+ via an abiotic pathway (surface adsorption and struvite crystallization), mitigating NH_3 emissions by 21.29–27.99%, while upregulating nitrification genes (*amoA*, *hao*, *nxrA*) and enriching functional consortia (*Bacillaceae*) to enhance total nitrogen retention (by 3%) through a biotic pathway. The biotic-abiotic synergy elevated the humification index ($P_{V,n}/P_{III,n}$) by 24.01–33.61%. The potential mechanism might be that a nitrogen retention supplied nitrogen skeleton and nitrogenous precursors for aromatic condensation reactions. Moreover, the enriched functional microbiota (*Thermobifida*) drove lignin degradation and protein-like conversion, redirecting toward precursors to stable humic-like substances. The phosphorus mainly mediated and enhanced the humification process (+ 7.74% vs. BCPM), while magnesium synergistically reduced more NH_3 emissions (–8.51% vs. BCP). Therefore, based on the phosphorus-magnesium co-modified biochar, increasing the phosphorus content loaded on biochar offers greater potential for humification. The spatiotemporal coordination of abiotic mineral interactions and biotic microbial specialization enabled simultaneous nitrogen retention and humification in composting.

Highlights

- P/P-Mg modified biochar synchronously boosts nitrogen retention and humification via biotic-abiotic mechanisms.
- Functional microbiota redirect nitrogenous organics to humic substances formation.
- Biochar-microbe synergy establishes a dual-functional framework for sustainable composting additive design.

*Correspondence:
Jing Yuan
jingyuan@cau.edu.cn
Full list of author information is available at the end of the article

Keywords Phosphorus and magnesium modified biochar, Composting, Ammonia emission, Humification, Biotic-abiotic mechanisms

Graphical Abstract

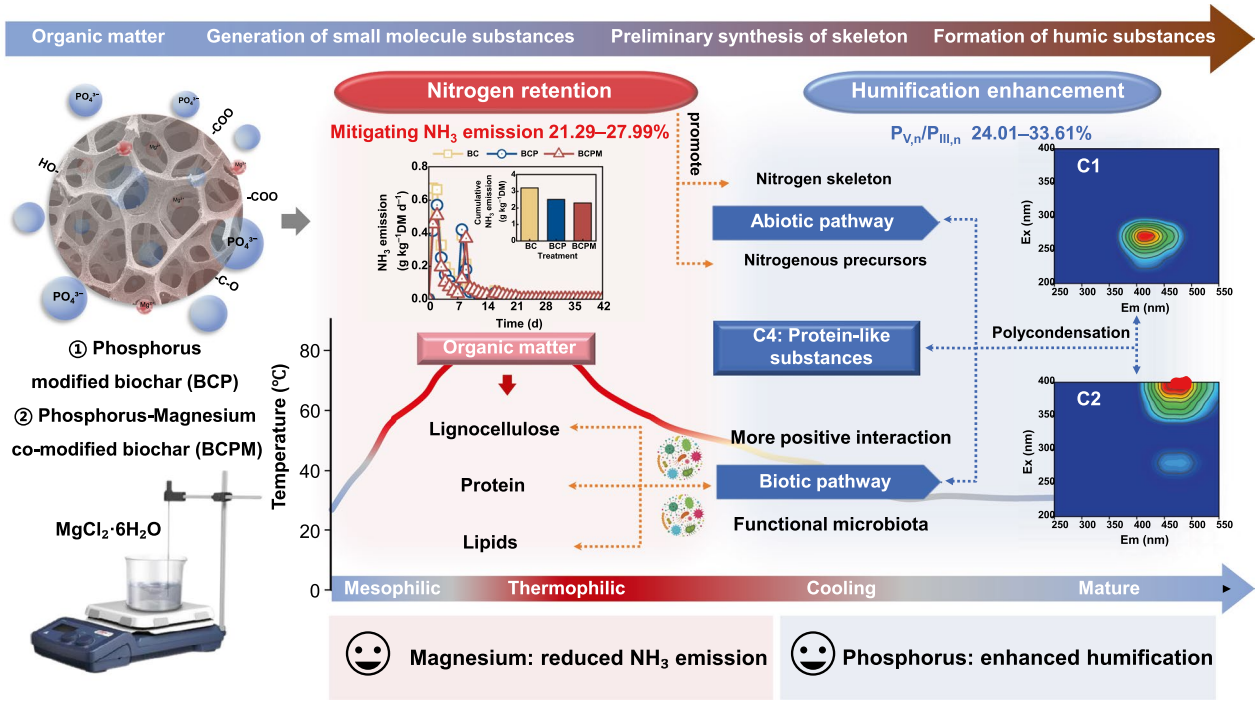

1 Introduction

Composting serves as a critical technological bridge for converting organic waste into humus-rich fertilizers, advancing circular agriculture and sustainable development (Zhao et al. 2022a). However, conventional composting faces two persistent challenges: substantial nitrogen loss (16–74% of initial nitrogen via NH_3 volatilization) (Cáceres et al. 2018; Liu et al. 2023a, b) and inefficient humification, which limits its soil application potential (Chen et al. 2023a). Moreover, humic substances (HS), as the cornerstone of compost quality, require nitrogen participation in biological and abiotic humification pathways (Li et al. 2025; Xu et al. 2022). Dual enhancement of nitrogen conservation and humification efficiency remains unresolved.

Phosphate-magnesium (P-Mg) salts have emerged as promising additives, reducing NH_3 emissions by 69.4% and total nitrogen loss by 60.6% through struvite crystallization (Zhao et al. 2020). Phosphate additives also accelerate abiotic humification by promoting complex HS structures (Yang et al. 2024), while magnesium-phosphate fertilizers enhance humification via mineral release (Kong et al. 2022a). Therefore, P-Mg salts constitute promising additives for the concurrent optimization of humification efficiency and emission mitigation. However, high-dose P-Mg salt application (10–20% dry weight) triggers salt stress (EC > 4 mS cm^{-1}), causing phytotoxicity (Chan et al. 2016; Jiang et al. 2016; Shan et al. 2021) and suppressing microbial activity, thereby compromising composting efficiency.

To resolve this issue, biochar emerges as a synergistic carrier. Its inherent properties could mitigate NH_3 loss and salt stress (Guo et al. 2020), while modified biochars (MBC) further overcome limitations of conventional biochar (e.g., limited adsorption capacity and insufficient surface active site density) through tailored functionalization (Ravindiran et al. 2024). For instance, iron-modified biochar enhances nitrogen retention in composting systems via synergistic surface chemisorption and microbiome modulation (Tang et al. 2025). Qiu et al. (2025) demonstrated that phosphoric acid-modified biochar accelerates sewage sludge humification. Gu et al. (2025) engineered magnesium-modified biochar to reduce NH_3 emissions by 18% via pore-functionalization. However,

these single-element modified biochars fail to analyze the nitrogen–humification trade-off and underlying mechanisms during composting, while the effect of P-Mg co-modified biochar's dual-functional enhancement remains unexplored during composting.

Recent advances highlight inseparable linkages between compost humification and N transformation, prompting intensified investigation into their synergy. Recent advances confirm that optimized nitrogen sources enhance biodegradability and humification efficiency (Lin et al. 2024). Furthermore, Liu et al. (2023a) demonstrated that as the precursors for humification, the releasing of biogenic N-containing compounds from sludge is important for controlling humification. Nitrogen scarcity during compost maturation constrains microbial metabolism and humic acid polymerization (Wang et al. 2023a, b). Phosphate additives in compost have been shown to enrich functional microbial communities to promote the formation of humic acid carbon and nitrogen skeletons (Su et al. 2024). Modified biochars could physically adsorb nitrogen while biologically activating microbiota, offering dual pathways to enhance composting humification and nitrogen retention. Specifically, surface-loaded ions provide active sites for abiotic NH_4^+ fixation, forming a biochar composite carrier through microbial regulation. On the other hand, the composite carrier simultaneously provides humification precursors and microbial niches for both biological and abiotic pathways. Despite its potential, critical knowledge gaps persist regarding: How does P-Mg salt-modified biochar coordinate abiotic fixation and biological regulation under composting stress to achieve dual nitrogen-humification enhancement?

This study systematically investigates the mechanisms by which P-Mg salt-modified biochar coordinates biological and abiotic pathways to enhance nitrogen retention and humification in swine manure composting. By integrating tracking of nitrogen transformation, fluorescence spectroscopy, functional genomics, and microbial succession dynamics, we aim to elucidate the interplay between P-Mg salt-modified biochar mediated nitrogen conservation and humification processes. Our findings provide a novel strategy for developing advanced composting additives that concurrently improve fertilizer quality and environmental sustainability in waste management.

2 Materials and methods

2.1 Composting materials

The raw materials were fresh pig manure, woodchips, and cornstalk. Pig manure was collected from the Sujiatuo Pig Farm (Haidian District, Beijing, China). The cornstalk was taken from the Shangzhuang Experimental Station of China Agricultural University (Haidian District, Beijing, China) and crushed into 2–5 cm particles. The wood chips were taken from a furniture processing factory (Hebei) and the particle size was 1–3 mm. Key physiochemical properties of composting materials are shown in Table S1. Biochar made from wood chips was purchased from Henan Lize Environmental Protection Technology Co., Ltd. The pyrolysis temperature of biochar was 500 ℃. The particle size of the biochar was 100 mesh, its organic carbon content was 68%, its pH value was 9.00, its moisture content was 10.35%, and its ash content was 9.45%. The modified biochar samples were prepared using the impregnation method (Tang et al. 2025; Wang et al. 2023a). Briefly, the biochar was rinsed with deionized water for surface impurities and dried at 60 ℃ for 24 h. According to a previous study by Jiang et al. (2016) and Wu et al. (2017), the addition of phosphorus (P) and magnesium (Mg) salts at 20% (molar mass) of the initial nitrogen content is appropriate. 100 g of biochar was immersed in 0.59 mol L^{-1} KH_2PO_4 (analytical pure-grade) solution, and the reaction was carried out at 25 ℃ with magnetic stirring at 150 r min^{-1} for 3 h. The soaked biochar was washed with deionised water until the pH of the filtrate was maintained, and then dried at 60 °C for 24 h. The product was cooled, crushed, sieved (0.15 mm), and labeled as conventional biochar (BC) or phosphorus-modified biochar (BCP) respectively. Phosphorus-magnesium co-modified biochar (BCPM) was prepared using BCP as a raw material in the same method, with impregnation using 0.59 mol L^{-1} $MgCl_2{\cdot}6H_2O$ solution.

2.2 Experimental system and protocols

Three composting experiments were performed at the Shangzhuang Experimental Station of China Agricultural University (Haidian District, Beijing, China). A stainless steel composting reactor with an effective volume of 60 L was used in this study. The parameters of this reactor have been reported elsewhere (Yuan et al. 2018).

The mixture of pig manure with woodchips and cornstalks (as bulking agents) was used as composting feedstock at a wet weight ratio of 17:2:1. The moisture content of the feedstock was set at 65% and the mixture weight was 35 kg. Multiple comparative trials suggest that 8–10% biochar addition (dry weight) achieves maximal nitrogen conservation efficiency and phosphorus bioavailability (Wang et al. 2021; Wei et al. 2016; Qian et al. 2013). Three treatments with the addition of 8% (dry weight) of BC, BCP and BCPM respectively were designed and were designated as "BC", "BCP" and "BCPM". The three treatments were consecutively operated for 6 weeks and the manual turning was conducted on days 7, 14, 21, 28, 35, and 42. The initial aeration rate was 0.24 L kg^{-1} DM min^{-1}. The aeration rate was reduced by 50% and 75% during the cooling and maturity periods,

respectively. Solid samples were collected from five representative points (including the top, middle and bottom parts of the compost pile and the inner and outer layers) in each reactor after manual turning, homogenized, and stored at –4 °C or –80 °C for physicochemical and microbiological analysis, respectively. Three technical replicates were analyzed per sample.

2.3 Analytic methods

2.3.1 Characterization of biochar materials

The specific surface area and pore structure of BC, BCP and BCPM were characterized using an automated specific surface and porosity analyzer (BET, Micromeritics ASAP 2460, USA). Fourier-transform infrared spectroscopy (FTIR) was employed to analyze the functional group composition of the biochar using a Thermo Scientific Nicolet iS20 spectrometer. A scanning electron microscope mirror (SEM, ZEISS Gemini 300, Germany) was used to analyze the surface morphology of the biochar. Energy Dispersive X-ray Spectroscopy (EDS) was used to analyze the surface chemistry of the biochar.

2.3.2 Physicochemical properties

The moisture content was measured by drying fresh solid samples at 105 °C for 12 h. Fresh solid samples were mixed with deionized water at a mass ratio of 1:10 and shaken for 30 min to obtain the water extract, which was used to measure electrical conductivity (EC), and germination index (GI). The EC values were determined with an EC meter (pHS-3C, Shanghai Precision & Scientific Instruments Co., Ltd., China). GI was measured using the method described previously by (Kong et al. 2022b; Wang et al. 2022b). Fresh solid samples were also extracted using 2 M potassium chloride (1:10, w/v) to determine the concentration of ammonium nitrogen (NH_4^+–N) and nitrate nitrogen (NO_3^-–N) using a flow analyzer (Technicon Auto Analyzer3; Seal Analytical GmbH, Norderstedt, Germany). A solution of 2% boric acid and 0.1 M sulphuric acid were utilized to absorb and titrate NH_3 for quantification, respectively. Elemental contents contents were determined using an elemental analyzer (vario MACRO cube, Ele mentar, Hanau, Germany). Nutrients (P, Mg and K) were determined by inductively coupled plasma–mass spectrometry (5800 ICP-OES, Agilent, USA).

2.3.3 EEM and PARAFAC modeling

EEM fluorescence spectra of the fractions were obtained using a Hitachi F-7000 fluorescence spectrophotometer (Hitachi High Technologies, Japan). The excitation wavelengths (Ex) were 200 – 600 nm at 10 nm intervals and the emission wavelengths (Em) were 200 – 600 nm at 1 nm intervals. The EEM spectra of Milli-Q water were obtained and subtracted as the background of the EEM spectra of all the samples in order to minimise the effect of Rayleigh scattering and Raman scattering. The measured fluorescence intensities are given in Raman Units (R.U.). All samples were diluted with the same dissolved organic carbon (DOC) content to compare EEM spectra. The EEM spectrum was divided horizontally and vertically into five regions. Aromatic protein-like substances were represented by regions (I) and (II), fulvic-acid-like substances by region (III), soluble-microbial-byproduct-like substances by region (IV), and humic-acid-like substances by region (V) (Chen et al. 2003). EEM spectra were analyzed using fluorescence region integration (FRI) to evaluate the distribution of organic matter.

PARAFAC analysis was carried out in MATLAB 2018a (Mathworks, Natick, MA) with the DOMFluor toolbox (www.models.life.ku.dk), according to the tutorial of Stedmon (Stedmon and Bro 2008). Component identification was conducted through the OpenFluor online spectral library (https://openfluor.lablicate.com), which catalogs auto-fluorescence spectra of environmental organic compounds (Murphy et al. 2014). The humification index (HIX) was computed as H/(L + H), where H and L are the integrated emission intensities in the ranges of 435–480 nm and 300–345 nm, respectively, under an excitation of 254 nm. These two areas are calculated between emission wavelengths 300 nm and 345 nm for L and between 435 and 480 nm for H. The biogenic index (BIX) is calculated at λ_{exc} 310 nm, by dividing the fluorescence intensity emitted at λ_{em} 380 nm, by the fluorescence intensity emitted at λ_{em} 430 nm (Huguet et al. 2009).

2.3.4 High-throughput sequencing

To reveal the microbial succession, DNA was extracted from the composting samples collected on 0, 7, 21 and 42 day. Each sample was analyzed in three replicates. DNA was extracted by utilizing the AxyPrep DNA Isolation Kit (AXYGEN Inc., United States). The high-throughput sequencing was performed with the Illumina HiSeq PE3000 platform (Shanghai Majorbio Bio-Pharm Technology Co., Ltd, Shanghai). The PCR primers 338F and 806R targeting the 16S rRNA gene V3-V4 field were used to investigate the response of composting bacteria to different biochar.

2.3.5 Quantitative PCR of genes

The total genomic DNA for detecting genes and 16S rRNA was extracted using the FastDNA Spin Kit for Soil (MP Biomedicals) following the manufacturer's instructions. Nitrogen genes (*amoA*, *hao*, *nxrA*) and 16S rRNA were quantified by the WaferGen SmartChip Real-Time qPCR System (WaferGen Bio-systems, Fremont, CA, USA). Primers (Table S2) from previous

studies (Liu et al. 2024) and from Anhui Microanaly Genetech Co., Ltd were employed for amplification.

2.4 Statistical analysis

In this study, the mean values and standard deviations of the triplicate measurements for each treatment are reported. Statistics were analysed with SAS 8.2 (SAS Institute, Cary, NC, USA) and SPSS 26.0 (IBM, USA). OriginPro 2024 and Adobe Illustrator 2021 software were used to generate graphs. Differential bacteria between different treatments were identified using a three-group comparison and Linear Discriminant Analysis Effect Size (LEfSe). Moreover, bacterial functions were predicted based on the Functional Annotation of Prokaryotic Taxa (FAPROTAX) database. An interactive Mantel test correlation heatmap was generated using the ChiPlot online website (https://www.chiplot.online/).

3 Results and discussion

3.1 Characterization of biochar

The efficacy of biochar in composting systems is intrinsically linked to its structural and compositional characteristics (An et al. 2022). Phosphorus (P) loading on the biochar (4.22% in BCP, 3.45% in BCPM) induced surface roughening and particle irregularity (Fig. 1A–C), resulting in reduced specific surface area (Table 1). Furthermore, BCPM exhibited additional magnesium (Mg) enrichment (0.88%) compared to BCP, as confirmed by EDS elemental mapping and quantitative elemental detection (Fig. 1D–G). Although direct XRD or XPS speciation was not performed, prior studies confirm that KH_2PO_4-modified biochars retain predominantly bioavailable orthophosphates and condensed phosphates (Huang et al. 2023). Despite the lower P concentration in BCPM compared to BCP, the synergistic interaction between P and Mg could further improve nitrogen fixation efficiency. Notably, the total amount of P and Mg

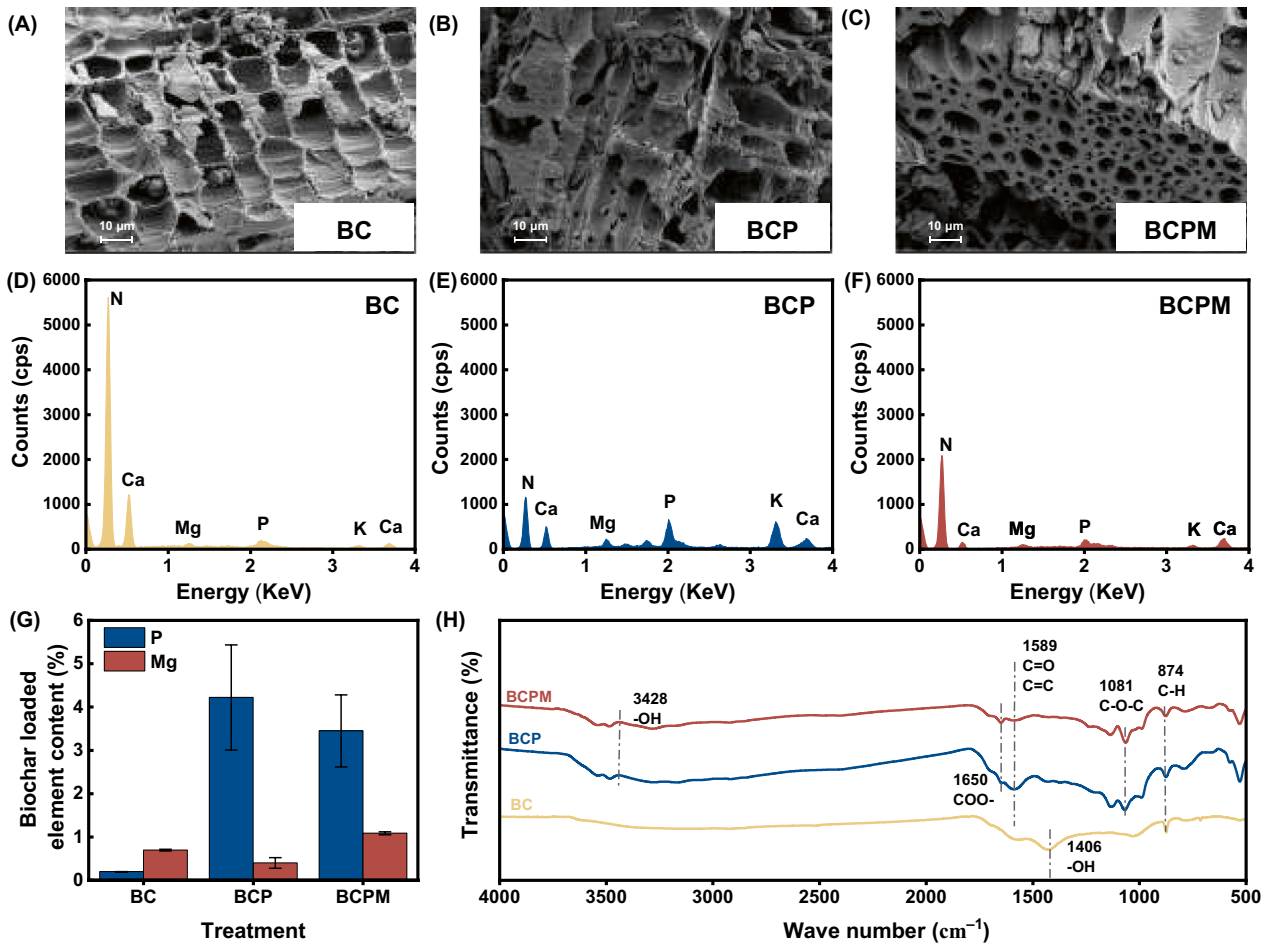

Fig. 1 Scanning Electron Microscopy (SEM) images of BC (**A**), BCP (**B**) and BCPM (**C**); Energy Dispersive X-ray Spectrometer (EDS) images of BC (**D**), BCP (**E**) and BCPM (**F**); **G** P and Mg element content; **H** Infrared spectra. BC, BCP and BCPM represent conventional biochar (BC), phosphorus-modified biochar (BCP) and phosphorus-magnesium co-modified biochar (BCPM), respectively

Table 1 Basic physicochemical properties of biochar

Treatments	SSA	APD	TPV	pH	EC	Element			
	($m^2\ g^{-1}$)	(nm)	($cm^3\ g^{-1}$)	(-)	($mS\ cm^{-1}$)	C (%)	N (%)	H (%)	S (%)
BC	10.97	4.06	0.0111	8.23	0.71	48.76	0.99	3.16	0.21
BCP	5.61	8.06	0.0116	6.86	4.55	42.84	0.88	2.68	0.16
BCPM	5.01	9.30	0.0120	6.99	4.47	39.39	0.82	2.75	0.15

The specific surface area (SSA), average pore diameter (APD) and total pore volume (TPV)

BC, BCP and BCPM represent conventional biochar (BC), phosphorus-modified biochar (BCP) and phosphorus-magnesium co-modified biochar (BCPM), respectively

was approximately the same for BCP (4.62%) and BCPM (4.54%). FTIR analysis revealed that phosphate salt and magnesium salt modifications introduced oxygen-containing (C=O, C–O, –OH) and acidic (COO^-) functional groups, enhancing NH_4^+ adsorption capacity through the provision of active sites (Li et al. 2019; Wang et al. 2022c). In comparison to BC, BCP and BCPM introduced P/Mg and new functional groups, which resulted in alterations to the properties of biochar.

3.2 Physicochemical parameters of compost

All three treatments exhibited superior rapid warming performance, reaching the thermophilic stage (> 55 °C) on the first day (Fig. 2A). This phenomenon was attributed to the ability of biochar to enhance the metabolic efficiency of microorganisms, thereby facilitating the rapid decomposition of organic matter (OM) for heat production during composting. Modified biochars maintained thermophilic conditions (> 55 °C) for 18 days without compromising compost safety. Following a period of 21 days, the BCP and BCPM treatments exhibited accelerated cooling into the maturity phase. This facilitates the formation of humus from small molecules that are disintegrated during the thermophilic phase.

The composting process was observed to demonstrate opposing trends in oxygen concentration and temperature (Fig. 2B). The trend of oxygen concentration was consistent across treatments, with oxygen content gradually decreasing and then increasing again after turning. Reduced aeration (cut 50% on day 9; cut 75% on day 22) caused transient oxygen fluctuations during thermophilic phases. Oxygen levels remained above 5% throughout the composting process to maintain aerobic microbial activity (Zeng et al. 2016).

The electrical conductivity (EC) value affects the quality of the compost as well as its potential phytotoxicity. The EC demonstrated a declining and then ascending trend (Fig. 2E). The final EC of the three treatments reached a plateau at approximately 2.4 mS cm^{-1}, below the the phytotoxicity threshold (4 mS cm^{-1}). It is worth noting that the addition of phosphate and magnesium salts to the compost resulted in high conductivity values, even exceeding phytotoxicity threshold (Chan et al. 2016). However, the addition of BCP and BCPM was observed to mitigate this phenomenon. This mitigation arose from NH_4^+ immobilization via struvite crystallization and surface adsorption (Jiang et al. 2016).

The seed germination index (GI) presented a fluctuating upward trend (Fig. 2F). GI values of the treatments reached the highest values on the 35th day (BC: 107.61%; BCP: 124.19%; BCPM: 133.86%), driven by the reduction of phytotoxic substances (e.g., volatile fatty acids, NH_4^+) and humus formation (Wang et al. 2020). The final GI decreased significantly (reaching 85.81–94.87%), which was correlated with salt ion accumulation during the maturity period. However, the final GI values of BCP and BCPM were increased by 1.42% and 10.57%, respectively, relative to BC. This may be related to the fact that phosphorus and magnesium are key nutrients required by plants in biological processes, including enzyme activity, protein synthesis, photosynthesis and seed germination (Wang et al. 2022b). It is also likely that BCP and BCPM promote humification.

3.3 Nitrogen transformation

The nitrogen transformation dynamics revealed distinct patterns in NH_4^+ and NO_3^- evolution (Fig. 3A, B). All treatments exhibited a predominant trajectory of initial NH_4^+ accumulation followed by progressive depletion, despite slight divergence in BC during days 28–35 (Fig. 3A). During thermophilic phases, NH_4^+ accumulation stemmed from enhanced organic nitrogen mineralization mediated by ammonifying microbiota (Awasthi et al. 2017). Subsequently, as the temperature decreased, the NH_4^+ content also declined, which may be associated with the resumption of nitrification (Zhang et al. 2019) This was also supported by the fact that a significant increase in NO_3^- content could be observed on the 35th day of composting. At the end of composting, the NO_3^- content of BCP and BCPM was significantly increased by 87 and 88 times, respectively, compared to BC (5.21 mg kg^{-1}DM). NH_4^+ content was consistently higher in BCP and BCPM than in BC. NH_4^+ accumulation in BCP and BCPM compost increased by 32.84% and 23.06%,

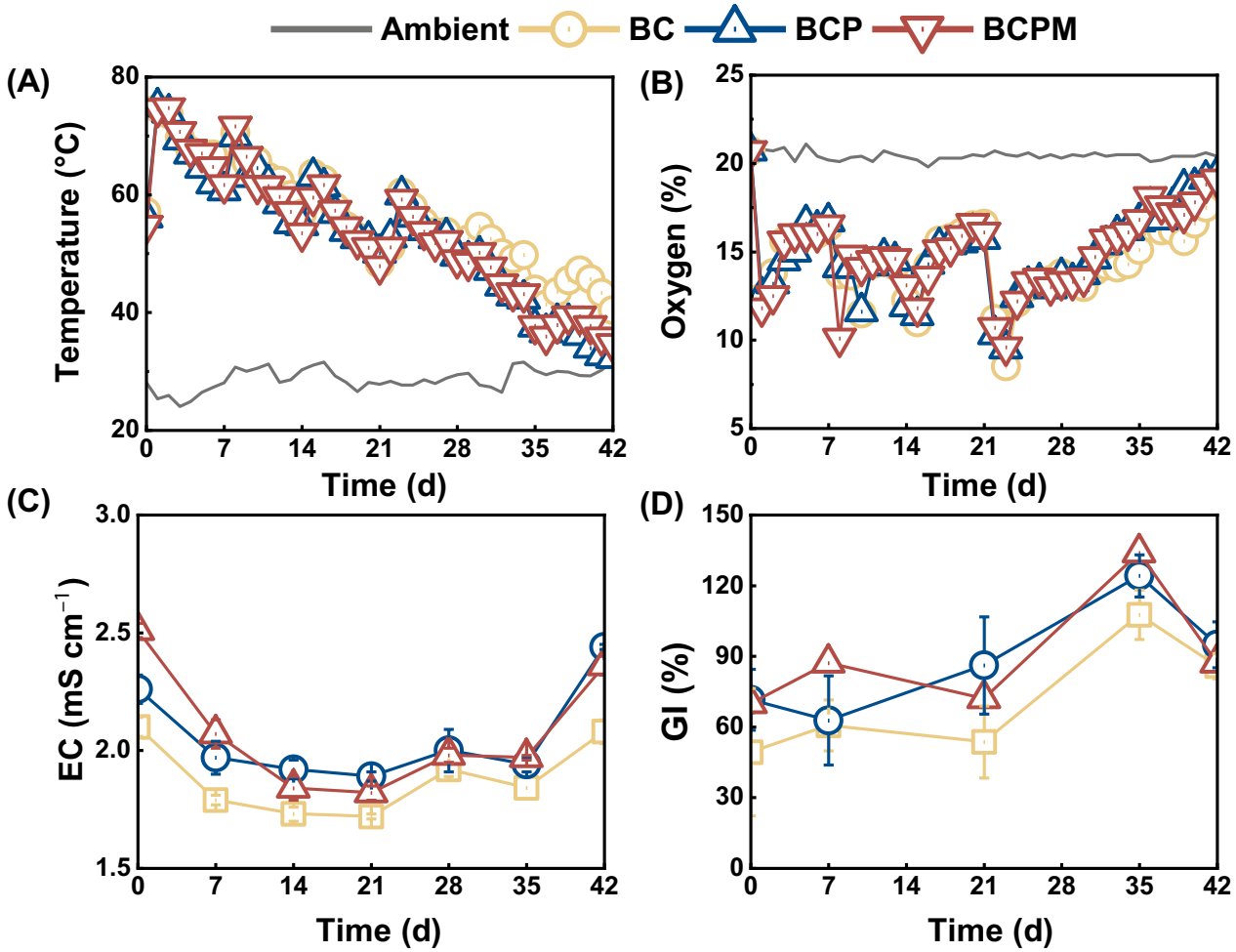

Fig. 2 Temporal changes in the **A** temperature, **B** oxygen content, **C** electrical conductivity (EC) and **D** germination index (GI) during pig manure composting. BC, BCP and BCPM represent treatments with the addition of conventional biochar (BC), phosphorus-modified biochar (BCP) and phosphorus-magnesium co-modified biochar (BCPM), respectively

respectively. Similar results were found in the study by Jiang et al. (2016), where the addition of magnesium salts and phosphates was able to increase the $NH_4^+$and NO_3^- concentrations.

The mineralisation of organic nitrogen to NH_4^+ and subsequent conversion to NH_3 could occur under conditions of high temperature and alkaline pH. All treatments exhibited substantial NH_3 emissions during the thermophilic phase, with peak emission rates recorded at 0.67, 0.57, and 0.51 g kg^{-1}DM d^{-1} for BC, BCP, and BCPM, respectively, during the initial week (Fig. 3C). Notably, the emission differential between treatments diminished in the second week as pH levels stabilized.

Compared to BC, BCP and BCPM demonstrated superior NH_3 mitigation performance, reducing cumulative emissions by 21.29% and 27.99%, respectively. This enhancement was attributed to a surface adsorption through oxygen-containing functional groups (C=O, COO^-) that immobilized NH_4^+ (Zhu et al. 2023). Surface charge modifications played distinct roles. In BCP, phosphorus loading increased surface negative charge (from P-containing groups), enhancing electrostatic attraction of NH_4^+ in the composting pH environment (7.5–9.0). In BCPM, magnesium loading (via Mg^{2+} sites) reduced net negative charge (Ibrahim et al. 2024), further strengthening NH_4^+ adsorption. Crucially, Mg^{2+} enabled struvite formation, co-immobilizing NH_4^+ and PO_4^{3-} during composting (Ren et al. 2009). Notably, Gu et al. (2025) reported an 18% reduction in NH_3 using Mg-modified biochar alone, whereas our BCPM achieved a significantly higher reduction of 27.99%. This disparity underscores phosphate's indispensable role in forming struvite ($MgNH_4PO_4$). These mechanisms accounted for BCPM's additional 8.51% NH_3 emission mitigation compared to BCP, underscoring the role of magnesium-phosphate synergy.

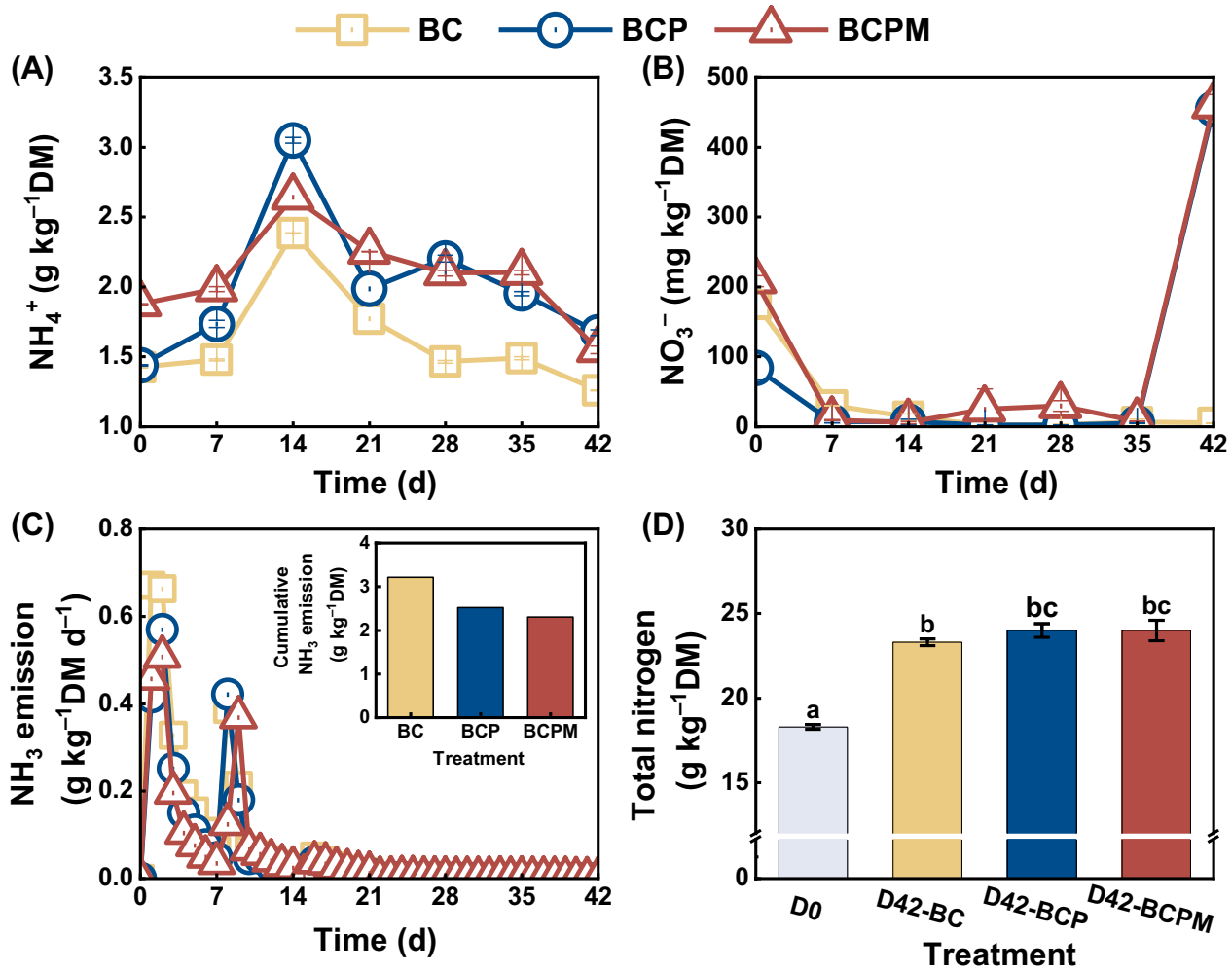

Fig. 3 Changes in **A** ammonia nitrogen (NH_4^+–N), **B** nitrate nitrogen (NO_3^-–N), **C** NH_3 daily and cumulative emissions and **D** total nitrogen during composting. BC, BCP and BCPM represent treatments with the addition of conventional biochar (BC), phosphorus-modified biochar (BCP) and phosphorus-magnesium co-modified biochar (BCPM), respectively

More importantly, total nitrogen (TN) increased by 27.32–31.15% across treatments (Fig. 3D), with BCP/BCPM achieving 3% higher TN retention than BC, demonstrating effective reconciliation of NH_4^+ and NO_3^- accumulation and nitrogen loss mitigation. The parity in TN levels despite BCPM's lower NH_3 emissions implies nitrogen redistribution, where BCP was likely to stabilize more nitrogen via humus complexation. Meanwhile, due to the physical concentration effect and biotransformation (Yang et al. 2019), total phosphorus (TP) and total potassium (TK) were significantly higher in BCP (13.42% and 12.00%) and BCPM (20.00% and 15.50%) compared to BC (Table 2). It resulted in an increase in total nutrients by 9.96% and 14.27% for BCP and BCPM, respectively. Given the phosphorus modification in both BCP and BCPM, Olsen-P content serves as a critical indicator of compost fertilizer efficiency. Compared to BC, BCP and BCPM elevated Olsen-P levels by 26.84% and 32.48%, respectively (Table S3). Modified biochar likely enhances the dissolution of sparingly soluble inorganic phosphates and mineralization of organic phosphorus, thereby increasing bioavailable phosphorus pools (Cui et al. 2022). Thus, BCP and BCPM demonstrated superior nutrient retention and supply capacity as safe and effective amendments.

3.4 Humification variations and pathways

Regulating nitrogen sources enhanced humification efficiency (Lin et al. 2024), as evidenced by multi-spectral analysis in this study. EEM spectroscopy coupled with Fluorescence Regional Integration (FRI) revealed distinct phase-dependent humus evolution patterns (Fig. 4A, B). All treatments exhibited consistent fluorescence shifts: decreased soluble microbial by-products (region IV) and

Table 2 Total nutrients before and after composting

Treatment	D0				D42			
	TN	TP	TK	Total	TN	TP	TK	Total
BC	18.3	25.8	15.0	59.1	23.3	38.0	20.0	81.3
BCP	18.3	28.6	16.8	63.8	24.0	43.1	22.4	89.4
BCPM	18.3	28.5	16.4	63.2	24.0	45.6	23.3	92.9

Total nitrogen (TN), total phosphorus (TP) and total potassium (TK). All values are expressed as g kg^{-1} on a dry weight basis

BC, BCP and BCPM represent treatments with the addition of unmodified biochar (BC), phosphorus-modified biochar (BCP) and phosphorus-magnesium co-modified biochar (BCPM), respectively

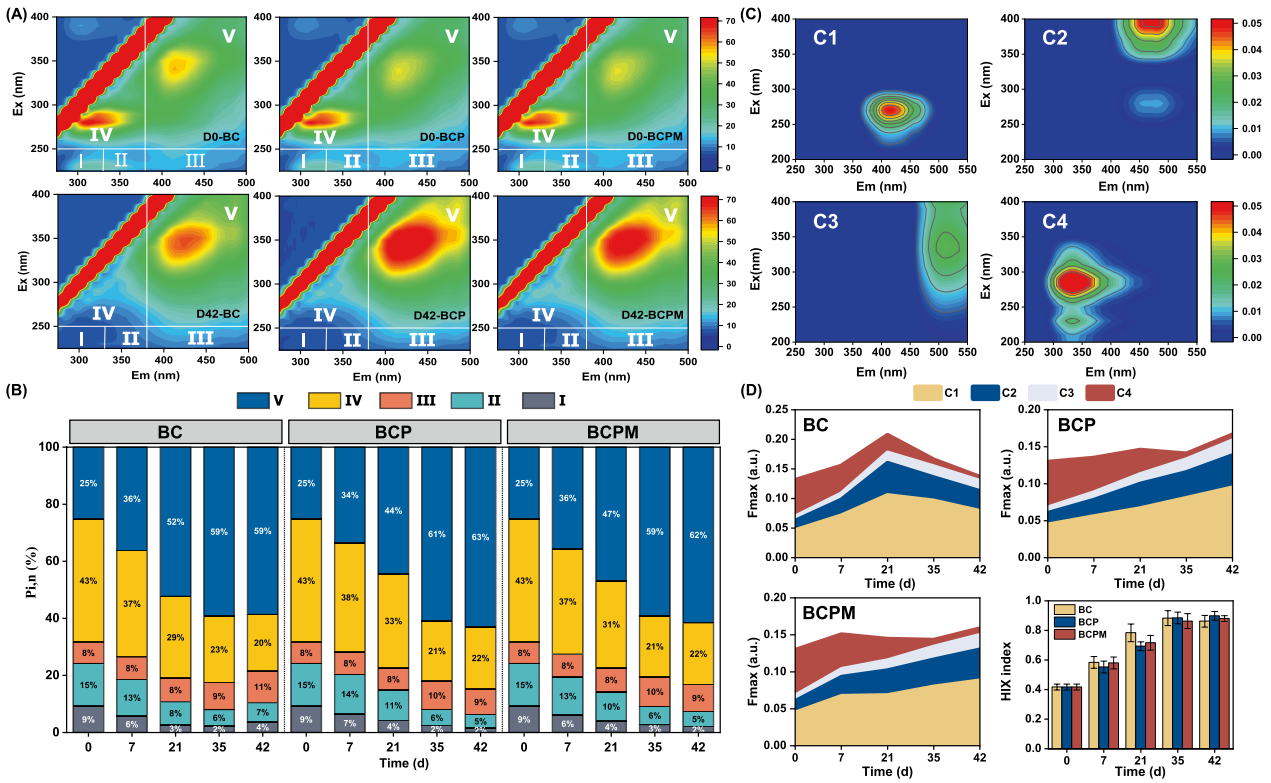

Fig. 4 **A** Excitation-emission matrix spectra of initial mixture and final compost of different treatments; **B** Distribution of fluorescence regional integration from samples (region I: aromatic protein-like substances, region II: aromatic protein-like substances, region III: fulvic acid-like substances, region IV: soluble microbial by-product-like substances, region V: humic-like substances); **C** Three fluorescent components decomposed by the PARAFAC model according to the EEMs of humic acid samples; **D** Distribution of three PARAFAC-derived components. *Fmax (a.u.)* represents the maximum fluorescence intensity (arbitrary units)

increased humic-like substances (region V) during the 42 days of composting. Notably, BCP and BCPM achieved 33.61% and 24.01% higher $P_{V,n}/P_{III,n}$ ratios than BC, indicating enhanced humic acid polymerization. These findings align with previous reports on phosphate-enhanced humus stabilization (Kong et al. 2022a; Liu et al. 2022). This also explained the higher GI of BCP and BCPM. Elevated phosphorus levels may accelerate organic matter decomposition and humic acid polymerization by activating lignin-degrading microbes and serving as electron acceptors for phosphate respiration. Thus, BCP (P:4.22%) was superior to BCPM (P:3.45%) in promoting humification by 7.74%.

EEM-PARAFAC can be applied to identify fluorescent components of protein-like and humic substances (HS) in dissolved organic matter and efficiently reflect the humification process. EEM-PARAFAC decomposition identified four fluorescent components (Fig. 4C). C1 and C2 were humic-like substances (Jutaporn et al. 2020; Liu et al. 2019; Ren et al. 2021),

C3 was fulvic-acid substances (Chai et al. 2019), and C4 was protein-like/amino acid-like (Kim et al. 2020). F_{max} percentages may indicate changes in fluorescent fraction concentrations. Temporal F_{max} variations revealed critical process dynamics (Fig. 4D). All treatments exhibited gradual enrichment of stable humic components (C1–C2) concurrent with C4 depletion, confirming the conversion of protein-like precursors into aromatic humic structures (Jutaporn et al. 2020; Yu et al. 2019). The complexity of compost feedstock properties dictates that humic acid formation typically involves synergistic interactions between multiple abiotic and biotic pathways (Wei et al. 2022). BCP and BCPM exhibited comparable compositional trends that diverged markedly from BC, suggesting distinct humification pathways between the treatments.

Specifically, in the BC group, F_{max} values of all components peaked on day 21 before declining. This indicated that the humic acid precursor substances synthesised in BC were unstable and biodegradable. This transient accumulation pattern was corroborated by the biological index (BIX) (Fig. S1A), reflecting the dominance of unstable biogenic substances. Conversely, BCP and BCPM exhibited progressive accumulation of humic-like (C1–C2) and fulvic-like (C3) substances, achieving final ratios of 0.16 and 0.15 respectively, surpassing BC's 0.13. This is consistent with the previous results for GI and EC. Notably, BCP/BCPM increased humic acid nitrogen (HA-N) by 41.99–44.44% over BC, peaking at day 35 (Fig. S2). This aligns with humification dynamics and ammonia-nitrite succession patterns. These results confirmed the immobilization of nitrogen into humic matrices. Phosphate-magnesium modified biochar could enhance humification through dual pathways. On the one hand, immobilized NH_4^+ (23–33% higher than BC) provided nitrogenous skeletons for aromatic condensation (Zhang et al. 2021), as evidenced by $SUVA_{254}$ increases (Fig. S1B). On the other hand, adding phosphate enriched phosphate-solubilizing microbiota, driving nitrogen utilization efficiency to accelerate humus precursors formation (Wei et al. 2021). Microbiota-driven protein-like components (C4) degradation supplied precursors for humic acid polymerization (Gao et al. 2024). The humification index (HIX) confirmed these synergistic effects again, with final values reaching 0.90 (BCP) and 0.88 (BCPM) compared to 0.86 for BC (Fig. 4D). This 2.07–4.22% enhancement demonstrates that phosphate-magnesium co-modification or phosphate modification optimally coordinates abiotic precursor supply with biotic polymerization processes, establishing an efficient pathway for humus formation.

3.5 Microbial community succession during composting

Microorganisms play a pivotal role in the biochemical process of composting, driving the transformation and stabilization of organic matter. The principal coordinate analysis (PCoA) based on Bray–Curtis distance elucidated the microbial community succession, with PC1 (41.18%) and PC2 (25.92%) explaining treatment-specific divergence (Fig. 5A). BCP and BCPM accelerated community succession, particularly during thermophilic (day 7) and cooling (day 21) phases, with convergence patterns emerging during maturation as temperature decreased.

Initial communities were dominated by Firmicutes (88.16%) and Bacteroidota (10.67%), collectively constituting > 95% of sequences (Fig. 5B). Thermophilic-phase oxygenic conditions favored functional Firmicutes genera (e.g. *Corynebacterium* and *Bacillus*) driving protein/lignocellulose degradation (Liu et al. 2023c). Actinobacteriota, critical for recalcitrant organic matter decomposition (Gladkov et al. 2022), increased markedly during thermophilic phases (28–39% abundance). BCP treatment outperformed BC and BCPM in enriching Actinobacteriota (31.14% and 39.64% in thermophilic and cooling phases, respectively), correlating with enhanced humus precursor accumulation. The results corroborated BCP's optimal humification performance. Notably, Actinobacteriota and Chloroflexi (enriched in BCP/BCPM during humification) synergistically mediated phosphate-regulated nitrogen transformation and humic acid synthesis, consistent with established humification pathways (Wang et al. 2022a, b).

LEfSe analysis identified stage-specific biomarkers regulated by modified biochar (Fig. 5C). BCPM enriched thermophilic-phase biomarkers (*Bacillus*, *Tepidimicrobium*) that enhanced NH_3 mitigation, while promoting *Corynebacterium*-mediated depolymerization of organics into humic acid precursors (e.g., amino acids, reducing sugars, and polyphenols). BCP and BCPM treatments uniquely enriched *Terrisporobacter* and *Clostridium_sensu_stricto_1* for organic degradation, alongside *Ammoniibacillus* to reduce nitrogen loss during the cooling phase (Wei et al. 2022). In contrast, *Thermoclostridium* and *Planifilum* were prevalent in the BC treatments (8.88% and 4.24%, respectively), exhibiting ammonia-oxidizing activity that likely exacerbated nitrogen loss through volatilization (Hoang et al. 2022). During the cooling and maturation phase, BCP and BCPM selectively enriched cellulolytic genera (*Thermobifida*, *Saccharomonospora*), synergistically enhancing biotic-abiotic lignocellulose-to-humus conversion (Zhang et al. 2023). These phosphate-magnesium co-modification or phosphate modification optimized core microbial succession, demonstrating dual benefits in humification promotion and nitrogen retention.

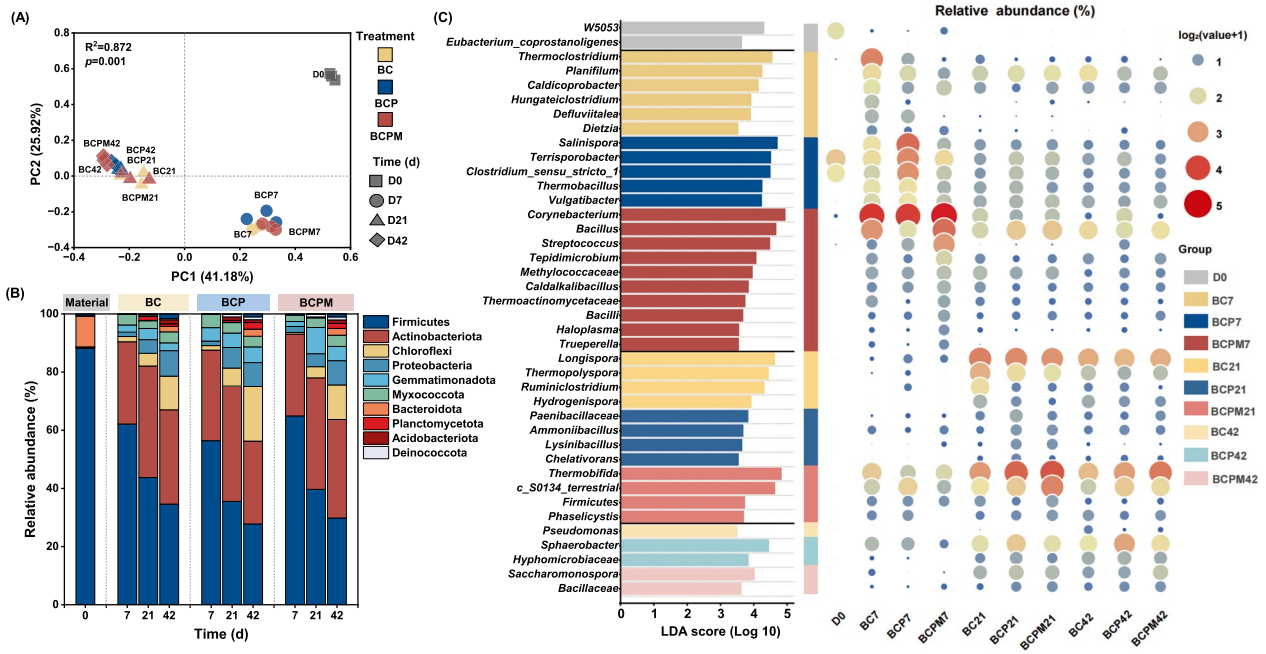

Fig. 5 **A** β-diversity (indicated by PCoA based on Bray–Curtis); **B** Dominant bacterial community at the phylum level (relative abundance > 1%) during composting; **C** Linear discriminant effect size (LEfSe) analysis to screen biomarkers at the genus level from bacterial community and their relative abundance at different stages of composting ($p > 0.05$). BC, BCP and BCPM represent treatments with the addition of conventional biochar (BC), phosphorus-modified biochar (BCP) and phosphorus-magnesium co-modified biochar (BCPM), respectively.

3.6 Functional microbial metabolism during composting

qPCR-based quantification of nitrifying genes (*amo*A, *hao* and *nxr*A) elucidated their mediation of nitrogen cycling toward humification pathways (Fig. 6). The abundance of nitrification genes exhibited a progressive increase, indicating enhanced nitrification activity that aligned with NO_3^- accumulation trends (Chen et al. 2023a, b; Liu et al. 2023c). Nitrogen transformation mediated by functional microorganisms may indirectly regulate humus formation (Tian et al. 2024). Ammonia-oxidizing bacteria (AOB) catalyze the conversion of NH_4^+-N to NO_2^--N through *amoA*-encoded ammonia monooxygenase, thereby stimulating microbial biosynthesis (e.g., *Bacillaceae*) to drive humus formation. Thus, *amo*A gene dynamics are critically linked to nitrogen cycling and humification (Xu et al. 2022). The absolute abundance of the *amo*A gene in the BCP and BCPM groups was found to exceed that of the BC group (Fig. 6A), which was attributed to the fact that BCP and BCPM provided sufficient substrate (NH_4^+) to AOB by BCP and BCPM. Correspondingly, *Bacillaceae* taxa (a humification-associated biomarker) in BCP and BCPM increased by 125% and 158% during the cooling phase, and 53% and 76% during the maturation phase compared to BC, facilitating the degradation of protein-like substances (C4 fraction) for humic precursor synthesis (Huang et al. 2022). The *hao* gene, encoding hydroxylamine oxidoreductase (HAO), governs the energy-yielding oxidation of hydroxylamine critical for AOB proliferation (Wu et al. 2012). Its temporal expression pattern paralleled that of *amo*A, with suppressed activity during thermophilic phases and subsequent activation in cooling stages. Subsequent nitrite oxidation mediated by *nxr*A completed the nitrification cascade. Despite BCPM exhibiting 12.43-fold higher *nxr*A abundance than BCP at maturity, no significant NO_3^--N divergence was observed, likely due to competitive NO_3^- utilization between *nxr*A-harboring microbes and denitrifiers (Duan et al. 2024). Strong inter-gene correlations (*amo*A, *hao*, *nxr*A; $p < 0.05$) suggest synergistic regulation of nitrogen transformation networks, potentially redirecting nitrogenous compounds toward humic precursor synthesis.

FAPROTAX annotation elucidated metabolic functions associated with nitrogen cycling and organic matter decomposition (Fig. 7A, B). Biochar amendments induced phase-specific functional differentiation within microbial consortia. Nitrogen-related functions (e.g., nitrogen fixation, nitrite ammonification, nitrate respiration) accounted for 0.18–2.53% of total annotations, with elevated activity during thermophilic (day 7) and maturation phases (day 42) corresponding to NH_4^+ and NO_3^- peaks. BCP and BCPM enhanced nitrogen-metabolizing

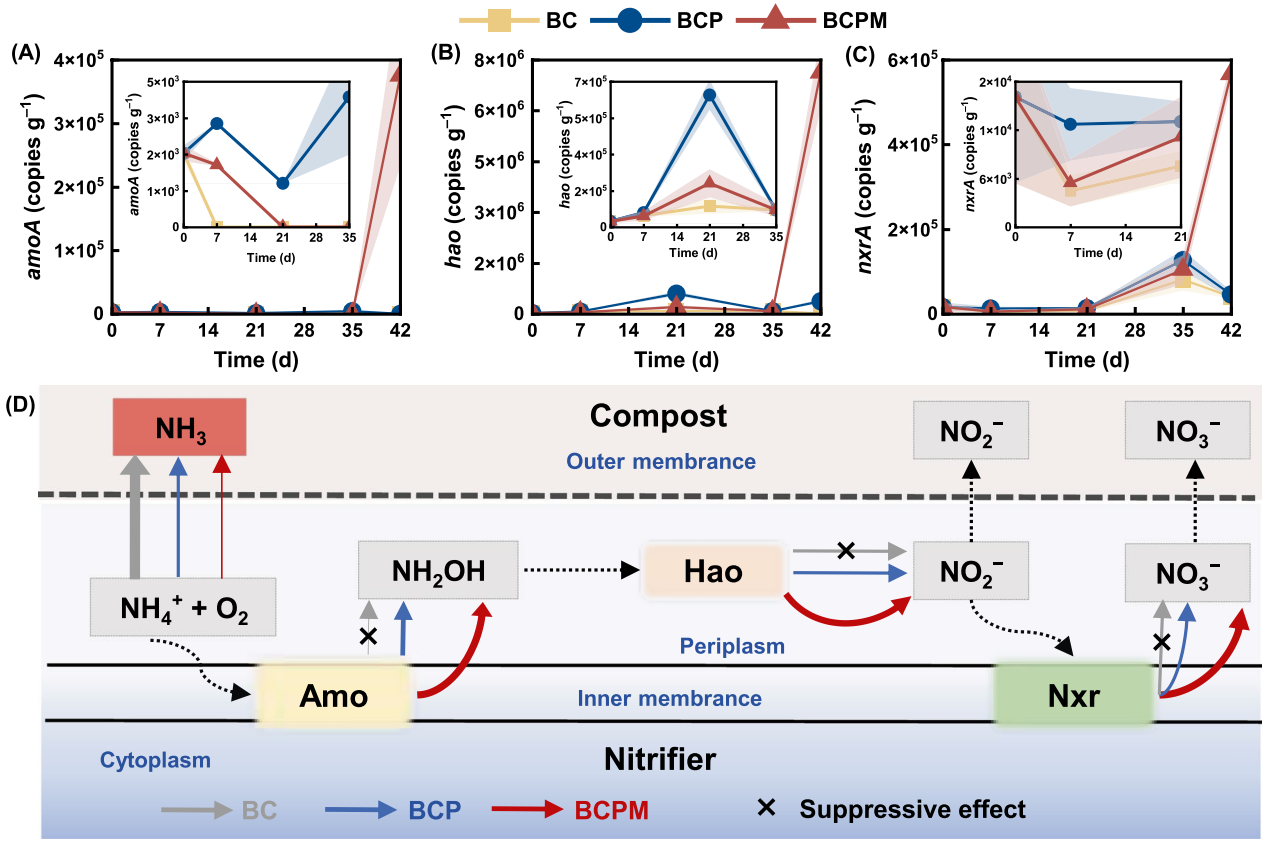

Fig. 6 Nitrogen cycle pathways in composting: **A**–**C** Abundance dynamics of nitrification genes (*amo*A, *hao*, *nxr*A) and **D** Nitrification processes

populations by 57% and 77% during thermophiles, and 22% and 14% at maturity compared to BC, corroborating gene-level results above. BCPM significantly amplified nitrogen respiration during the cooling phase. This process was potentially mediated by the keystone genus *Thermobifida*, which enhances microbial cooperation via positive cohesion effects to facilitate cellulose degradation (Zhao et al. 2022b). Organic degradation functions (cellulolysis, xylanolysis, ligninolysis) significantly increased and then decreased (0.08–17.12%), reflecting the gradual decrease of readily degradable organic matter. BCP and BCPM treatments selectively enhanced cellulolytic and xylanolytic capacities during cooling and maturation phases, thereby enriching humification precursors. Overall, BCP and BCPM optimized microbial functionality to synergistically improve nitrogen retention and humification efficiency in composting systems.

3.7 Mechanisms for synergistic nitrogen-humification enhancement

The Mantel test established a correlation network among core microbiota and composting performance (physicochemical factors, nitrogen transformation, and humification), elucidating the multi-scale regulatory mechanisms of BCP and BCPM in composting (Fig. 7C). Temperature, as a key physicochemical factor, significantly influenced the dynamics of TN and humic components (C1, C2, C3) ($p < 0.05$). TN showed a significant positive correlation with humic components (C1, C2, C3) and the humification index (HIX) ($p < 0.05$). These results further demonstrated that BCP/BCPM established a hierarchical biotic-abiotic pathway to redirect nitrogenous organics toward humification. BCP/BCPM immobilizes NH_4^+ via chemisorption by oxygen-containing functional groups and struvite crystallization. Enriched functional consortia (e.g., *Bacillaceae* and *Thermobifida*) degrade protein-like substances (C4 depletion) and lignin, generating nitrogenous precursors (amino acids, polyphenols). Subsequently, biochar, as an electron shuttle, facilitate redox reactions, integrating N-precursors into humic substances (C1/C2 components) via Maillard reactions and phenol–protein coupling (Fan et al. 2024; Yuan et al. 2017), elevating HA-N (Fig. S2) and HIX (0.88–0.90).

This process was supported by FAPROTAX annotation results, confirming the synergy between biotic and abiotic fixation. Notably, microbial communities showed significant positive correlations with NH_3 emissions and humic components ($p < 0.05$). Actinobacteria enriched

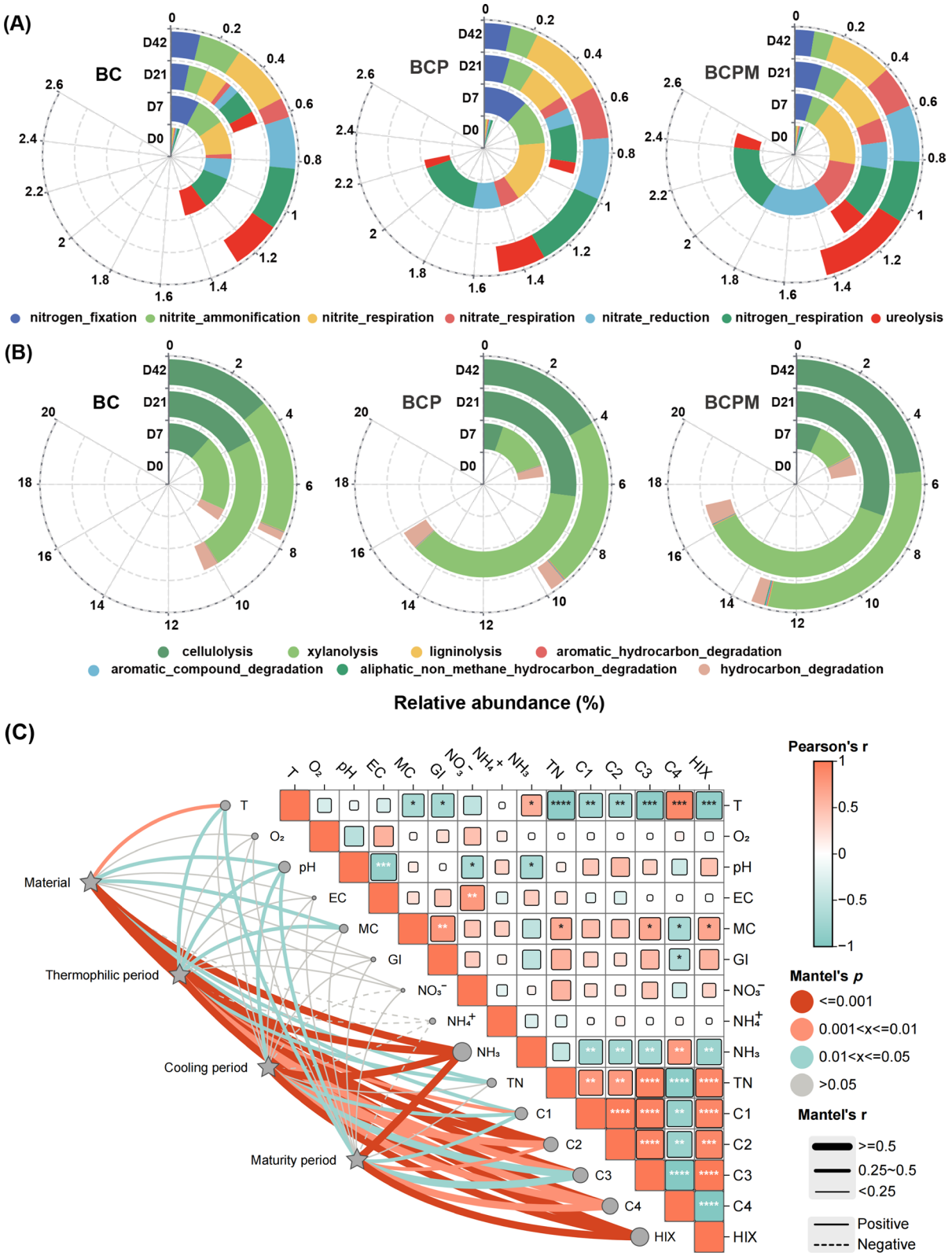

Fig. 7 Variation of main metabolic function profiles of bacterial community during composting analyzed by FAPROTAX: **A** Nitrogen cycling and **B** Organic matter decomposition. **C** Mantel test of core microbiota and composting performance (physicochemical factors, nitrogen transformation, and humification)

during the thermophilic phase drove lignin degradation to generate polyphenol precursors, while the dominant genus *Thermobifida* in the cooling phase facilitated C4 to C1/C2 conversion via cellulase secretion. This phase-specific microbial succession was closely linked to BCP/BCPM-mediated microenvironment regulation: BCP/BCPM maintained localized higher PO_4^{3-} or Mg^{2+} concentrations through mesoporous confinement, promoting struvite crystallization (abiotic nitrogen fixation), while providing a nitrogen skeleton and humic acid precursors for functional microbiota to optimize precursor allocation (directing more protein-like/amino acid-like substances into humic-like substances). Moreover, functional nitrifying genes (*amoA*, *hao*, *nxrA*) orchestrate ammonia-to-nitrate oxidation, generating bioavailable N intermediates that indirectly fuel humification through microbial anabolism of polyphenol-protein complexes (Wu et al. 2020). These findings demonstrate that BCP/BCPM synchronously enhances nitrogen retention and humification efficiency by coordinating a hierarchical pathway of "biotic -abiotic".

This study establishes a mechanistic framework for mitigating nitrogen loss and enhancing humification efficiency in composting systems through phosphorus-modified or phosphorus-magnesium co-modified biochar. Despite comparable total P + Mg content in BCP (4.62%; P:4.22%, Mg:0.88%) and BCPM (4.54%; P:3.45%, Mg:1.09%), the superior nitrogen retention in BCPM (8.51% lower NH_3 emissions vs BCP) and enhanced humification in BCP (7.74% higher efficiency vs BCPM) indicate a synergistic allocation of functions. Based on the phosphorus-magnesium co-modified biochar, increasing the phosphorus content loaded on biochar would have a higher potential for humification. Co-optimization of P and Mg in composting systems is recommended to harness their synergistic potential. Future research should prioritize optimizing biochar P/Mg loading ratios to maximize synergistic effects to advance nutrient-efficient management of organic waste.

4 Conclusion

This study elucidated the mechanisms by which phosphorus (P) and phosphorus-magnesium (P-Mg) co-modified biochar synergistically enhance nitrogen retention and humification during composting through biotic-abiotic interplay. Abiotically, BCP and BCPM immobilized NH_4^+ via surface functional groups (C=O and COO^-) and struvite crystallization with PO_4^{3-}/Mg^{2+}, mitigating NH_3 emission and increasing nitrogen retention. Biotically, these amendments enriched keystone bacteria (e.g., *Thermobifida*, *Bacillaceae*) and upregulated nitrifying genes (*amoA*, *hao*, *nxrA*), facilitating nitrogen conversion, while boosting functional microbiota to drive protein-like precursor polymerization into humic substances. Crucially, nitrogen skeletons enabled aromatic condensation via Maillard reactions and phenol–protein coupling, while functional microbes supplied humic precursors through lignocellulose degradation. By integrating functional microbiota-material co-design, this study establishes a multi-scale regulatory framework for P/P-Mg biochar mediated composting, thereby advancing precision nutrient management in organic waste upcycling.

Supplementary Information

The online version contains supplementary material available at https://doi.org/10.1007/s42773-025-00530-7.

Additional file 1.

Acknowledgements
We would like to thank Meggie Biotechnology Ltd. for providing microbial sequencing services.

Author contributions
Ruolan Tang: Writing—original draft, Visualization, Software, Methodology, Formal analysis, Data curation, Conceptualization. Yan Liu: Data curation and Formal analysis. Jingyuan Ma: Data curation. Sheng Yao: Data curation. Tianyu Ren: Data curation. Xiaoyan Gong: Writing-review & editing, Supervision. Guoxue Li: Funding acquisition. Ruonan Ma: Writing-review & editing. Jing Yuan: Writing-review & editing, Validation, Supervision, Software, Methodology, Conceptualization. All authors read and approved the final manuscript.

Funding
This research was supported by the National Key R&D Program of China (2023YFD1702004), National Natural Science Foundation of China (42207380) and the 2115 Talent Development Program of China Agricultural University.

Data availability
All data generated or analyzed during this study are included in this published article and its additional files.

Declarations

Competing interests
The authors declare that they have no known competing financial interests or personal relationships that could have appeared to influence the work reported in this paper.

Author details
[1]State Key Laboratory of Nutrient Use and Management, Beijing Key Laboratory of Farmland Soil Pollution Prevention and Remediation, College of Resources and Environmental Sciences, China Agricultural University, Beijing 100193, China. [2]Organic Recycling Institute (Suzhou) of China Agricultural University, Wuzhong District, Suzhou 215128, China.

Received: 11 May 2025 Revised: 2 October 2025 Accepted: 7 October 2025
Published online: 10 February 2026

References

An T, Chang Y, Xie J, Cao Q, Liu Y, Chen C (2022) Deciphering physicochemical properties and enhanced microbial electron transfer capacity by magnetic biochar. Bioresour Technol 363:127894

Awasthi MK, Wang Q, Chen H, Wang M, Ren X, Zhao J et al (2017) Evaluation of biochar amended biosolids co-composting to improve the nutrient transformation and its correlation as a function for the production of nutrient-rich compost. Bioresour Technol 237:156–166
Cáceres R, Malińska K, Marfà O (2018) Nitrification within composting: a review. Waste Manag 72:119–137
Chai L, Huang M, Fan H, Wang J, Jiang D, Zhang M et al (2019) Urbanization altered regional soil organic matter quantity and quality: insight from excitation emission matrix (EEM) and parallel factor analysis (PARAFAC). Chemosphere 220:249–258. https://doi.org/10.1016/j.chemosphere.2018.12.132
Chan MT, Selvam A, Wong JWC (2016) Reducing nitrogen loss and salinity during 'struvite' food waste composting by zeolite amendment. Bioresour Technol 200:838–844. https://doi.org/10.1016/j.biortech.2015.10.093
Chen W, Westerhoff P, Leenheer JA, Booksh K (2003) Fluorescence excitation–emission matrix regional integration to quantify spectra for dissolved organic matter. Environ Sci Technol 37(24):5701–5710
Chen L, Chen Y, Li Y, Liu Y, Jiang H, Li H et al (2023a) Improving the humification by additives during composting: a review. Waste Manag 158:93–106. https://doi.org/10.1016/j.wasman.2022.12.040
Chen P, Cheng W, Li S (2023b) Optimization strategies for mitigating nitrogen loss in the aerobic composting of pig manure and microbial changes revealed by metagenomic analysis. Process Saf Environ Protect 169:270–284. https://doi.org/10.1016/j.psep.2022.11.014
Cui H, Ou Y, Wang L, Yan B, Li Y, Bao M (2022) Dissolved organic carbon, a critical factor to increase the bioavailability of phosphorus during biochar-amended aerobic composting. J Environ Sci 113:356–364. https://doi.org/10.1016/j.jes.2021.06.019
Duan X, Zhai W, Wang Y, Sun K, Wang X, Hao P et al (2024) Effects of adding exogenous microorganisms on nitrogen conversion and its mechanism of action in pig carcass composting. J Clean Prod 449:141734. https://doi.org/10.1016/j.jclepro.2024.141734
Fan B, Zhao C, Zhao L, Wang M, Sun N, Li Z et al (2024) Biochar application can enhance phosphorus solubilization by strengthening redox properties of humic reducing microorganisms during composting. Bioresour Technol 395:130329. https://doi.org/10.1016/j.biortech.2024.130329
Gao X, Zhang J, Liu G, Kong Y, Li Y, Li G et al (2024) Enhancing the transformation of carbon and nitrogen organics to humus in composting: biotic and abiotic synergy mediated by mineral material. Bioresour Technol. https://doi.org/10.1016/j.biortech.2023.130126
Gladkov GV, Kimeklis AK, Afonin AM, Lisina TO, Orlova OV, Aksenova TS et al (2022) The Structure of Stable Cellulolytic Consortia Isolated from Natural Lignocellulosic Substrates. Int J Mol Sci. https://doi.org/10.3390/ijms231810779
Gu X, Li H, Shi Y, Sun C, Li J, Li S (2025) Magnesium modified biochar facilitates favorable nitrogen conversion to mitigate ammonia and nitrous oxide emissions during pig manure composting. Chem Eng J 504:159073. https://doi.org/10.1016/j.cej.2024.159073
Guo X, Liu H, Zhang J (2020) The role of biochar in organic waste composting and soil improvement: a review. Waste Manage 102:884–899. https://doi.org/10.1016/j.wasman.2019.12.003
Hoang HG, Thuy B, Lin C, Vo D, Tran HT, Bahari MB et al (2022) The nitrogen cycle and mitigation strategies for nitrogen loss during organic waste composting: a review. Chemosphere. https://doi.org/10.1016/j.chemosphere.2022.134514
Huang W, Wen P, Wang W, Liu X, Wang Y, Yu Z et al (2022) Hydrothermal pretreatment improves humification in co-composting of oil palm fronds and paper mill sludge. J Environ Chem Eng 10(3):107985. https://doi.org/10.1016/j.jece.2022.107985
Huang K, Sun X, Sun J, Guo Y, Hu X, Hu C et al (2023) The role of phosphorus speciation of biochar in reducing available Cd and phytoavailability in mining area soil: effect and mechanism. Sci Total Environ 894:164868
Huguet A, Vacher L, Relexans S, Saubusse S, Froidefond JM, Parlanti E (2009) Properties of fluorescent dissolved organic matter in the Gironde Estuary. Org Geochem 40(6):706–719. https://doi.org/10.1016/j.orggeochem.2009.03.002
Ibrahim MM, Lin H, Chang Z, Li Z, Riaz A, Hou E (2024) Magnesium-doped biochars increase soil phosphorus availability by regulating phosphorus retention, microbial solubilization and mineralization. Biochar 6(1):68
Jiang T, Ma X, Yang J, Tang Q, Yi Z, Chen M et al (2016) Effect of different struvite crystallization methods on gaseous emission and the comprehensive comparison during the composting. Bioresour Technol 217:219–226. https://doi.org/10.1016/j.biortech.2016.02.046
Jutaporn P, Armstrong MD, Coronell O (2020) Assessment of C-DBP and N-DBP formation potential and its reduction by MIEX® DOC and MIEX® GOLD resins using fluorescence spectroscopy and parallel factor analysis. Water Res 172:115460. https://doi.org/10.1016/j.watres.2019.115460
Kim J, Kim T, Park SR, Lee HJ, Kim JK (2020) Factors controlling the distributions of dissolved organic matter in the East China Sea during summer. Sci Rep 10(1):11854
Kong Y, Ma R, Li G, Wang G, Liu Y, Yuan J (2022a) Impact of biochar, calcium magnesium phosphate fertilizer and spent mushroom substrate on humification and heavy metal passivation during composting. Sci Total Environ 824:153755. https://doi.org/10.1016/j.scitotenv.2022.153755
Kong Y, Wang G, Chen W, Yang Y, Ma R, Li D et al (2022b) Phytotoxicity of farm livestock manures in facultative heap composting using the seed germination index as indicator. Ecotoxicol Environ Saf 247:114251
Li X, Shi X, Yang Z, Xu X, Guo R (2019) Effects of recyclable ceramsite as the porous bulking agent during the continuous thermophilic composting of dairy manure. J Clean Prod 217:344–351. https://doi.org/10.1016/j.jclepro.2019.01.148
Li M, Jiang H, Li R, Liu W, Xie Y, Wu W et al (2025) Effects of biochar-loaded microbial agent in regulating nitrogen transformation and integration into humification for straw composting. Bioresour Technol 417:131873. https://doi.org/10.1016/j.biortech.2024.131873
Lin J, Mao Y, Mai L, Li G, Liu H, Peng S et al (2024) Accelerating the humification of mushroom waste by regulating nitrogen sources composition: deciphering mechanism from bioavailability and molecular perspective. Chemosphere 349:140816. https://doi.org/10.1016/j.chemosphere.2023.140816
Liu C, Du Y, Yin H, Fan C, Chen K, Zhong J et al (2019) Exchanges of nitrogen and phosphorus across the sediment-water interface influenced by the external suspended particulate matter and the residual matter after dredging. Environ Pollut 246:207–216. https://doi.org/10.1016/j.envpol.2018.11.092
Liu Y, Ma R, Tang R, Kong Y, Wang J, Li G et al (2022) Effects of phosphate-containing additives and zeolite on maturity and heavy metal passivation during pig manure composting. Sci Total Environ 836:155727. https://doi.org/10.1016/j.scitotenv.2022.155727
Liu J, Wang N, Fujii M, Bao Z, Wei J, Hao Z et al (2023a) Insights into the roles of DOM in humification during sludge composting: comprehensive chemoinformatic analysis using FT-ICR mass spectrometry. Chem Eng J 475:146024. https://doi.org/10.1016/j.cej.2023.146024
Liu Y, Tang R, Li L, Zheng G, Wang J, Wang G et al (2023b) A global meta-analysis of greenhouse gas emissions and carbon and nitrogen losses during livestock manure composting: influencing factors and mitigation strategies. Sci Total Environ 885:163900
Liu Z, Awasthi MK, Zhao J, Liu G, Syed A, Al-Shwaiman HA et al (2023c) Unraveling impacts of inoculating novel microbial agents on nitrogen conversion during cattle manure composting: core microorganisms and functional genes. Bioresour Technol 390:129887. https://doi.org/10.1016/j.biortech.2023.129887
Liu Y, Tang R, Liu G, Li G, Wang J, Cai Y et al (2024) Dicyandiamide addition delay nitrous oxide emission and shift its production pathway from denitrification to incomplete nitrification in maturation phase of composting. Chem Eng J 495:153225
Murphy KR, Stedmon CA, Wenig P, Bro R (2014) Openfluor– an online spectral library of auto-fluorescence by organic compounds in the environment. Anal Methods 6(3):658–661
Qian T, Zhang X, Hu J, Jiang H (2013) Effects of environmental conditions on the release of phosphorus from biochar. Chemosphere 93(9):2069–2075. https://doi.org/10.1016/j.chemosphere.2013.07.041
Qiu X, Feng M, Chen R, Chen J, Zheng X, Mao X et al (2025) Phosphoric acid modified biochar enhanced heavy metals passivation via accelerating humification and bioremediation in sewage sludge composting. Environ Technol Innov 39:104275. https://doi.org/10.1016/j.eti.2025.104275
Ravindiran G, Rajamanickam S, Janardhan G, Hayder G, Alagumalai A, Mahian O et al (2024) Production and modifications of biochar to engineered materials and its application for environmental sustainability: a review. Biochar 6(1):62

Ren L, Li G, Shen Y, Schuchardt F, Lu P (2009) Chemical precipitation for controlling nitrogen loss during composting. Waste Manage Res 28(5):385–394. https://doi.org/10.1177/0734242X09336546
Ren W, Wu X, Ge X, Lin G, Zhou M, Long Z et al (2021) Characteristics of dissolved organic matter in lakes with different eutrophic levels in southeastern Hubei Province, China. J Oceanol Limnol 39(4):1256–1276
Shan G, Li W, Gao Y, Tan W, Xi B (2021) Additives for reducing nitrogen loss during composting: a review. J Clean Prod 307:127308
Stedmon CA, Bro R (2008) Characterizing dissolved organic matter fluorescence with parallel factor analysis: a tutorial. Limnol Oceanogr Methods 6:572–579
Su J, Zhan Y, Chang Y, Chang S, Luo Y, Chen P et al (2024) Phosphate additives promote humic acid carbon and nitrogen skeleton formation by regulating precursors and composting bacterial communities. Bioresour Technol 399:130617. https://doi.org/10.1016/j.biortech.2024.130617
Tang R, Yao S, Liu Y, Ren T, Ma J, Gong X et al (2025) Iron-modified biochar enhanced nitrogen retention during composting:bridging chemisorption and microbiome modulation. Chem Eng J 513:162761. https://doi.org/10.1016/j.cej.2025.162761
Tian X, Qin W, Zhang Y, Liu Y, Lyu Q, Chen G et al (2024) The inoculation of thermophilic heterotrophic nitrifiers improved the efficiency and reduced ammonia emission during sewage sludge composting. Chem Eng J 479:147237
Wang G, Kong Y, Liu Y, Li D, Zhang X, Yuan J et al (2020) Evolution of phytotoxicity during the active phase of co-composting of chicken manure, tobacco powder and mushroom substrate. Waste Manag 114:25–32
Wang SP, Wang L, Sun ZY, Wang ST, Shen CH, Tang YQ et al (2021) Biochar addition reduces nitrogen loss and accelerates composting process by affecting the core microbial community during distilled grain waste composting. Bioresour Technol. https://doi.org/10.1016/j.biortech.2021.125492
Wang G, Kong Y, Yang Y, Ma R, Shen Y, Li G et al (2022a) Superphosphate, biochar, and a microbial inoculum regulate phytotoxicity and humification during chicken manure composting. Sci Total Environ 824:153958. https://doi.org/10.1016/j.scitotenv.2022.153958
Wang G, Yang Y, Kong Y, Ma R, Yuan J, Li G (2022b) Key factors affecting seed germination in phytotoxicity tests during sheep manure composting with carbon additives. J Hazard Mater 421:126809
Wang Y, Miao J, Saleem M, Yang Y, Zhang Q (2022c) Enhanced adsorptive removal of carbendazim from water by FeCl3-modified corn straw biochar as compared with pristine, HCl and NaOH modification. J Environ Chem Eng 10(1):107024
Wang J, Riaz M, Babar S, Xia H, Li Y, Xia X et al (2023a) Iron-modified biochar reduces nitrogen loss and improves nitrogen retention in Luvisols by adsorption and microbial regulation. Sci Total Environ 879:163196
Wang Y, Wei Y, Zhou K, Gao X, Chang Y, Zhang K et al (2023b) Regulating pH and *Phanerochaete chrysosporium* inoculation improved the humification and succession of fungal community at the cooling stage of composting. Bioresour Technol 384:129291. https://doi.org/10.1016/j.biortech.2023.129291
Wei Y, Zhao Y, Wang H, Lu Q, Cao Z, Cui H et al (2016) An optimized regulating method for composting phosphorus fractions transformation based on biochar addition and phosphate-solubilizing bacteria inoculation. Bioresour Technol 221:139–146. https://doi.org/10.1016/j.biortech.2016.09.038
Wei YQ, Wang J, Chang RX, Zhan YB, Wei D, Zhang L et al (2021) Composting with biochar or woody peat addition reduces phosphorus bioavailability. Sci Total Environ. https://doi.org/10.1016/j.scitotenv.2020.142841
Wei Y, Liang Z, Zhang Y (2022) Evolution of physicochemical properties and bacterial community in aerobic composting of swine manure based on a patent compost tray. Bioresour Technol 343:126136. https://doi.org/10.1016/j.biortech.2021.126136
Wu YC, Guo Y, Lin XG, Zhong WH, Jia ZJ (2012) Ihibition of bacterial ammonia oxidation by organohydrazines in soil microcosms. Front Microbiol. https://doi.org/10.3389/fmicb.2012.00010
Wu J, He S, Liang Y, Li G, Li S, Chen S et al (2017) Effect of phosphate additive on the nitrogen transformation during pig manure composting. Environ Sci Pollut Res Int 24(21):17760–17768
Wu J, Wei Z, Zhu Z, Zhao Y, Jia L, Lv P (2020) Humus formation driven by ammonia-oxidizing bacteria during mixed materials composting. Bioresour Technol 311:123500. https://doi.org/10.1016/j.biortech.2020.123500
Xu Z, Li R, Wu S, He Q, Ling Z, Liu T et al (2022) Cattle manure compost humification process by inoculation ammonia-oxidizing bacteria. Bioresour Technol 344:126314. https://doi.org/10.1016/j.biortech.2021.126314
Yang F, Li Y, Han Y, Qian W, Li G, Luo W (2019) Performance of mature compost to control gaseous emissions in kitchen waste composting. Sci Total Environ 657:262–269. https://doi.org/10.1016/j.scitotenv.2018.12.030
Yang X, Mazarji M, Li M, Li A, Li R, Zhang Z et al (2024) Mechanism of magnetite-assisted aerobic composting on the nitrogen cycle in pig manure. Bioresour Technol 391:129985
Yu Z, Liu X, Zhao M, Zhao W, Liu J, Tang J et al (2019) Hyperthermophilic composting accelerates the humification process of sewage sludge: molecular characterization of dissolved organic matter using EEM–PARAFAC and two-dimensional correlation spectroscopy. Bioresour Technol 274:198–206. https://doi.org/10.1016/j.biortech.2018.11.084
Yuan Y, Bolan N, Prévoteau A, Vithanage M, Biswas JK, Ok YS et al (2017) Applications of biochar in redox-mediated reactions. Bioresour Technol 246:271–281. https://doi.org/10.1016/j.biortech.2017.06.154
Yuan J, Li Y, Chen S, Li D, Tang H, Chadwick D et al (2018) Effects of phosphogypsum, superphosphate, and dicyandiamide on gaseous emission and compost quality during sewage sludge composting. Bioresour Technol 270:368–376
Zeng J, Shen X, Han L, Huang G (2016) Dynamics of oxygen supply and consumption during mainstream large-scale composting in China. Bioresour Technol 220:104–109. https://doi.org/10.1016/j.biortech.2016.08.070
Zhang L, Dong H, Zhang J, Chen Y, Zeng G, Yuan Y et al (2019) Influence of FeONPs amendment on nitrogen conservation and microbial community succession during composting of agricultural waste: relative contributions of ammonia-oxidizing bacteria and archaea to nitrogen conservation. Bioresour Technol 287:121463
Zhang Z, Wei Z, Guo W, Wei Y, Luo J, Song C et al (2021) Two types nitrogen source supply adjusted interaction patterns of bacterial community to affect humifaction process of rice straw composting. Bioresour Technol 332:125129. https://doi.org/10.1016/j.biortech.2021.125129
Zhang L, Shi T, Xu Z, Bao Z, Li J, Li G et al (2023) Effect of lime and calcium magnesium phosphate on gaseous emissions, maturity, and bacterial dynamics during food waste composting. Environ Technol Innov 32:103306. https://doi.org/10.1016/j.eti.2023.103306
Zhao S, Schmidt S, Qin W, Li J, Li G, Zhang W (2020) Towards the circular nitrogen economy—a global meta-analysis of composting technologies reveals much potential for mitigating nitrogen losses. Sci Total Environ 704:135401
Zhao S, Schmidt S, Gao H, Li T, Chen X, Hou Y et al (2022a) A precision compost strategy aligning composts and application methods with target crops and growth environments can increase global food production. Nat Food 3(9):741–752
Zhao Y, Weng Q, Hu B (2022b) Microbial interaction promote the degradation rate of organic matter in thermophilic period. Waste Manage 144:11–18
Zhu Y, Chen G, Yu D, Liu R, Chen X, Yang Z et al (2023) Sludge composting with self-produced carbon source by phosphate buffer coupled hyperthermophilic pretreatment realizing nitrogen retention. Chem Eng J 476:146811. https://doi.org/10.1016/j.cej.2023.146811